Doping-driven metal-insulator transitions and charge orderings in the extended Hubbard model

K. J. Kapcia,[1,*] S. Robaszkiewicz,[2] M. Capone,[3] and A. Amaricci[4]

[1]*Institute of Physics, Polish Academy of Sciences, Aleja Lotników 32/46, PL-02668 Warsaw, Poland*

[2]*Faculty of Physics, Adam Mickiewicz University in Poznań, ul. Umultowska 85, PL-61614 Poznań, Poland*

[3]*Scuola Internazionale Superiore di Studi Avanzati (SISSA), Via Bonomea 265, I-34136 Trieste, Italy*

[4]*Scuola Internazionale Superiore di Studi Avanzati and Democritos National Simulation Center, Consiglio Nazionale delle Ricerche, Istituto Officina dei Materiali, Via Bonomea 265, I-34136 Trieste, Italy*

(Received 11 November 2016; revised manuscript received 20 February 2017; published 9 March 2017)

We perform a thorough study of the extended Hubbard model featuring local and nearest-neighbor Coulomb repulsion. Using the dynamical mean-field theory we investigated the zero-temperature phase diagram of this model as a function of the chemical doping. The interplay between local and nonlocal interactions drives a variety of phase transitions connecting two distinct charge-ordered insulators, i.e., half filled and quarter filled, a charge-ordered metal and a Mott-insulating phase. We characterize these transitions and the relative stability of the solutions and we show that the two interactions conspire to stabilize the quarter-filled charge-ordered phase.

DOI: 10.1103/PhysRevB.95.125112

I. INTRODUCTION

Strongly correlated materials are characterized by the relevance of the Coulomb interaction which competes with the kinetic energy, leading to a tendency towards localization of the carriers [1,2]. The simplest theoretical description of this competition is obtained from the Hubbard model [3] in terms of conduction band electrons experiencing a *local* screened Coulomb repulsion. Despite its simplicity, the approximate solutions of this model revealed an incredibly rich physics which has been the object of extensive investigations (e.g., Refs. [4–9]). This model is also the starting point to take into account other important effects by including additional interactions, e.g., phonon coupling, orbital ordering, or longer-range interaction.

A great deal of attention has been devoted to understand the effects of nonlocal short-range electron-electron repulsion, which favors a spatial charge ordering [10]. The possible existence of inhomogeneous distribution of charges was first predicted in two-dimensional (2D) electron gas [11], as a result of the tendency to form a Wigner crystal as soon as the energy gain from the electronic localization tendency exceeds that in the kinetic energy for a homogeneous electron distribution. This possibility has been realized experimentally in various semiconductor structures [12–14]. The effective importance of the electronic interaction for the 2D electrons gas, e.g., layers of liquid helium, has been recently reconciled with the original Wigner crystallization scenario [15–17]. However, other, and somehow more conventional, examples of materials in which charge order interplays with Mott physics can be found in narrow-band correlated systems such as transition-metal dichalcogenides [18,19], or other oxides (e.g., manganites, nickelates, cuprates, bismuthates, and cobaltates) [20–24] as well as low-dimensional organic conductors [25–27] and heavy-fermion systems [28,29].

From a theoretical perspective all this evidence motivated a careful analysis of the extended Hubbard model (EHM), i.e., the Hubbard model supplemented with a *nonlocal* density-density interaction term. The direct competition of local and nonlocal interactions in the EHM captures both the effects of strong correlations and the tendency of the system to form inhomogeneous charge distributions. The EHM has been extensively studied in many different regimes, e.g., the strong-coupling limit, the quarter and half filling, and by means of different methods [30–32], such as the Hartree-Fock mean field [30,32–35], the Monte Carlo simulations [36–38], the variational-based cluster perturbation theory [39], the lattice exact diagonalization [40–43], the two-particle self-consistent approach [44], the density matrix renormalization group [45,46], as well as the dynamical mean-field theory [16,17,47–49] (DMFT) and its extensions [50–55].

A seminal study of the EHM within the DMFT has been reported in Ref. [47] for the quarter-filling case (i.e., for a total density $n = 0.5$). Using a combination of numerical tools the existence, at large values of the nonlocal interaction, of a charge-ordered phase separated from the Fermi liquid metal at weak coupling was demonstrated. The origin of such symmetry-broken state was interpreted in terms of the effect of strong correlation, signaled by the enhancement of the effective mass. For filling smaller than $n = 0.5$ and specific values of the local and nonlocal interactions the occurrence of phase separation between the Fermi liquid and the ordered phase has also been addressed in Ref. [48]. However, the existence of a genuine Mott-driven Wigner insulating state was demonstrated only later [16] in the quarter-filling regime. The study of the finite-temperature phase diagram revealed the existence of a strongly correlated charge-ordered metal, separating the Wigner-Mott insulator from the Fermi liquid phase [16,17]. The existence of a $T = 0$ charge-ordered metallic state at quarter filling has been also shown using cluster extension of the DMFT (CDMFT), which takes into account the role of short-ranged spatial correlation [50]. In particular, the onset of charge order was shown to be concomitant with the occurrence of short-range antiferromagnetism. More recently, the effects of nonlocal interaction have been studied in two- and three-dimensional cubic lattices using a combination of *GW* and the extended DMFT (*GW*+EDMFT) approach [51–53]. This approach enabled a systematic investigation of the screening effect and the role of longer-range interaction, up to the third-nearest-neighbors [53]. The solution the EHM

*konrad.kapcia@ifpan.edu.pl

 ©2017 American Physical Society

by means of the *GW*+EDMFT contributed to clarify the phase diagram of this model at and near the half-filling regime ($n = 1$) [53], associating the interplay between charge ordering and correlations with changes in the screening modes.

The emergence of charge order in strongly correlated systems is also largely affected by the geometric frustration factor, which in turn plays a relevant role in different systems, e.g., the charge-transfer salts θ-(BEDT-TTF)$_2$X or the dichalcogenide $1T$-TaS_2 both characterized by a triangular-lattice geometry. In this context the interaction-driven charge-ordered metal at quarter filling is associated with the emergence of a quantum phase, i.e., pinball liquid. This state is characterized by quasilocalized charges coexisting with more itinerant electrons, which gives rise to strong quasiparticle renormalization with a mechanism analogous to the heavy-fermion compounds [49]. In the multiorbital case [56], which is relevant for transition-metal oxides, the onset of a pinball phase has been associated with a finite value of the Hund's exchange [57].

Motivated by the experimental findings and the increasing theoretical work to understand the nature of strongly correlated electronic phases in the presence of charge ordering, in this paper we investigate the ground state properties of the EHM. We solve the model nonperturbatively using the DMFT, with a Lanczos-based exact diagonalization algorithm. We present a thorough investigation of the evolution of the phase diagram as a function of the local and nonlocal interaction for an arbitrary occupation of the system. We unveil the properties of the transitions among the multiple states characterizing the phase diagram of the system, in a full range of variation of the model parameters. In particular, we address the first- or second-order nature of the transitions separating the charge-ordered states from normal (disordered) phases. We study the behavior of the order parameter and other relevant quantities including the evolution of the spectral functions. By evaluating the grand canonical potential, we also determine the metastability of the solutions across the phase transitions and unveil the existence of phase separation on the phase diagram.

The rest of this paper is organized as follows. In Sec. II, we introduce the model and the method of solution. We also discuss the solution of the model in two limiting cases. In Sec. III we briefly present the half-filling $n = 1$ solution of the model and discuss the evolution of the phase diagram as a function of the chemical potential and for an increasing value of the interactions. In Sec. IV we present a detailed analysis for each phase transition occurring in the system. Finally, in Sec. V we summarize the results of this work and provide some future perspectives.

II. MODEL AND METHOD

We consider the EHM, which describes the effects of the Coulomb repulsion onto conduction band electrons in terms of local and nearest-neighbor density-density interactions. The model Hamiltonian reads

$$\hat{H} = -t \sum_{\langle i,j\rangle,\sigma} \hat{c}^{+}_{i\sigma}\hat{c}_{j\sigma} + U \sum_{i} \hat{n}_{i\uparrow}\hat{n}_{i\downarrow} + \frac{W}{2} \sum_{\langle i,j\rangle} \hat{n}_i\hat{n}_j - \mu \sum_{i} \hat{n}_i, \quad (1)$$

where $\langle i,j\rangle$ indicates summation over nearest-neighbor (NN) sites independently. The parameter t is the hopping amplitude, $\hat{c}^{+}_{i\sigma}$ ($\hat{c}_{i\sigma}$) denotes the creation (destruction) operator of an electron of spin $\sigma = \uparrow, \downarrow$ at site i. The operators $\hat{n}_i = \sum_\sigma \hat{n}_{i\sigma}$, $\hat{n}_{i\sigma} = \hat{c}^{+}_{i\sigma}\hat{c}_{i\sigma}$, denote the occupation number. Finally, μ is the chemical potential. The Hamiltonian terms proportional to U and W describe, respectively, the local and the nonlocal (NN) part of the screened Coulomb interaction. The competition between these two terms enables us to capture the interplay of strong correlation with charge ordering. In this work we focus on the checkerboard charge-ordered phases, which are known to be stable in the strong-coupling regime. For simplicity, we will not consider other textures, such as incommensurate ordering, which may become favored in the weakly interacting regime. Similarly, we will not consider magnetically ordered solutions, which could occur in this system in proximity to the half-filling regime, i.e., one particle per lattice site.

DMFT solution. We study the solution of model (1) using the DMFT [6]. In order to allow for a long-range charge-ordered phase (checkerboard type) the lattice is divided into two sublattices, indexed by $\alpha = A, B$. The DMFT approximation becomes exact in the limit of infinite coordination number $z \to +\infty$, provided that t and W are rescaled, respectively, as $t \to t/\sqrt{z}$ and $W \to W/z$ [17,58]. In this limit the nonlocal interaction term W is treated at the Hartree level [17,59]. After decoupling of the W term, Hamiltonian (1) takes the form

$$\hat{H}_{\mathrm{MF}} = -t \sum_{\langle i,j\rangle,\sigma} \hat{c}^{+}_{i\sigma}\hat{c}_{j\sigma} + \sum_{\alpha=A,B} \sum_{i\in\alpha} [U\hat{n}_{i\uparrow}\hat{n}_{i\downarrow} - (\mu - Wn_{\bar{\alpha}})\hat{n}_i] + C, \quad (2)$$

where $C = -\frac{1}{2}W(n^2 - \Delta^2)$ is a constant term, $\Delta = \frac{1}{2}(n_A - n_B)$ is the charge polarization, $n = \frac{1}{2}(n_A + n_B)$ is the total electron concentration, and n_α is the average density of the particles in each sublattice $\alpha = A, B$ ($n_\alpha = \frac{2}{L}\sum_{i\in\alpha}\langle\hat{n}_i\rangle$, L is the total number of the lattice sites). To fix ideas and to further simplify the treatment we shall consider the case of the Bethe lattice, characterized by a semielliptic density of states (per spin):

$$\rho_0(\epsilon) = \frac{2}{\pi D}\sqrt{1 - (\epsilon/D)^2} \quad \text{for} \quad |\epsilon| < D, \quad (3)$$

where $D = 2t$ is the half-bandwidth [or typical kinetic energy, $D = 2\sqrt{\int_{-\infty}^{+\infty}\epsilon^2\rho_0(\epsilon)d\epsilon}$]. In the following we set $D = 1$ as the energy unit. Section II B and Fig. 1(b), where we set $D = 0$, are exceptions of this general rule.

Within the DMFT the quantum many-body lattice problem (2) is mapped onto two distinct effective impurity problems, one per sublattice. The effective baths are described in terms of the frequency-dependent Weiss fields $\boldsymbol{\mathcal{G}}_0^{-1}(i\omega_n) = \mathrm{Diag}[\mathcal{G}_{0A}^{-1}(i\omega_n), \mathcal{G}_{0B}^{-1}(i\omega_n)]$, which are self-consistently determined by requiring to the impurity problems to reproduce the local physics of the lattice system. In this framework the self-energy matrix $\boldsymbol{\Sigma}(i\omega_n)$, describing the effects of interaction at the one-particle level, is approximated by its local part. For each sublattice the self-energy function is determined by the solution of the corresponding quantum impurity problem. In terms of the matrix self-energy the DMFT self-consistency

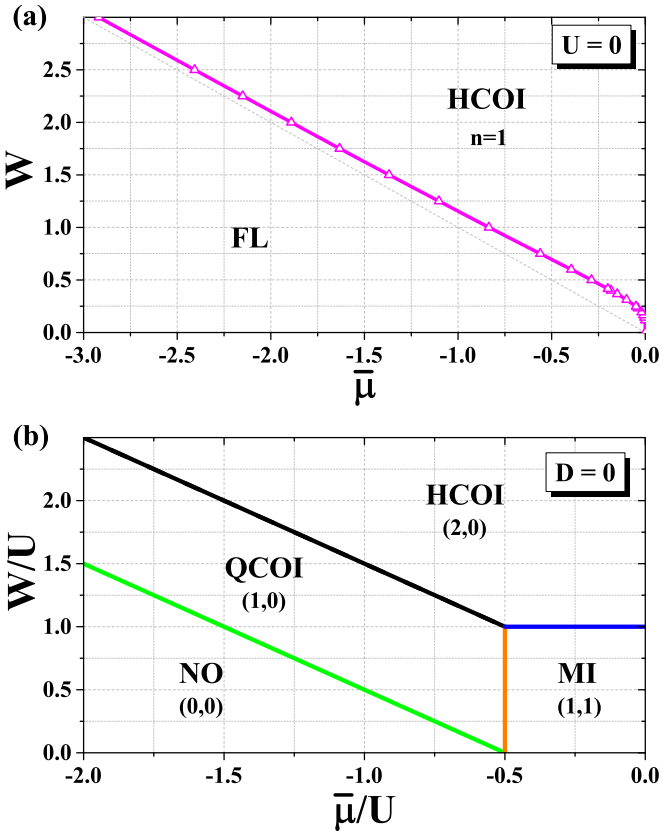

FIG. 1. (a) Phase diagram for $U = 0$ as a function of W and $\bar{\mu} = \mu - W/2$. The boundary between Fermi liquid (FL) and half-filled charge-ordered insulator (HCOI) is discontinuous. (b) Phase diagram for $D = 0$ (atomic limit) as a function of the interaction ratio W/U and $\bar{\mu}/U$, $\bar{\mu} = \mu - U/2 - W$. Each phase (NO, nonordered; MI, Mott insulator; QCOI, quarter-filled charge-ordered insulator; and HCOI) is labeled by values of (n_A, n_B). All the phases are insulating and all the boundaries are discontinuous.

condition reads

$$\mathcal{G}^{-1}(i\omega_n) = \boldsymbol{G}_{\rm loc}^{-1}(i\omega_n) + \boldsymbol{\Sigma}(i\omega_n), \tag{4}$$

where $\boldsymbol{G}_{\rm loc}$ is the diagonal matrix of the local interacting lattice Green's function. This equation relates the bath properties, expressed by the Weiss field, to the local physics of the lattice problem. In terms of the lattice density of states the components of the local Green's function are

$$G_{loc,\alpha}(i\omega_n) = \zeta_{\bar{\alpha}}(i\omega_n) \int \frac{\rho_0(\epsilon)d\epsilon}{\zeta_A(i\omega_n)\zeta_B(i\omega_n) - \epsilon^2}, \tag{5}$$

where $\alpha = A, B$ and $\zeta_\alpha(i\omega_n) = i\omega_n + \mu - Wn_{\bar{\alpha}} - \Sigma_\alpha(i\omega_n)$.

In this work we solve the effective quantum impurity problem using the exact diagonalization technique at $T = 0$, Refs. [60,61]. The effective bath is discretized into a finite number N_b of levels. The ground state of the corresponding Hamiltonian as well as the impurity Green's functions are determined using the Lanczos technique. Throughout this work we use $N_b = 9$, having checked the robustness of the results for $N_b = 8$ and $N_b = 0$. The whole DMFT algorithm proceeds as follow. For a given bath function $\mathcal{G}_0^{-1}$ the effective quantum impurity problems are solved. The resulting self-energy function $\boldsymbol{\Sigma}$ is used to determine the local interacting Green's function $\boldsymbol{G}_{\rm loc}$ by means of Eq. (5). Finally, using the self-consistency relation, Eq. (4), a new, updated Weiss field is obtained. The self-consistent DMFT equations are solved iteratively until the convergence is reached, usually in a few tens of iterations. A critical slowing down of the convergence can be observed near a phase transition.

In the following we restrict our attention to the case $U \geqslant 0$ and $W \geqslant 0$ and to the *nonmagnetic* phases. Furthermore, model (1) exhibits the particle-hole symmetry (for any U and W), so our results for $n \leqslant 1$ ($\bar{\mu} < 0$) are held identically also for $n > 1$ ($\bar{\mu} > 0$) (see, e.g., Ref. [34]). Finally, we checked that the occurring phases in this work are solutions with the lowest grand canonical potential (per site).

A. Noninteracting limit

For $U = 0$ ($W > 0$) model (2) is solved using a standard broken-symmetry Hartree-Fock approximation. The mean-field Hamiltonian is diagonalized by means of the Bogoliubov transformation [30,33,62–68]. The resulting self-consistent equations for the total occupation n and the charge polarization Δ are

$$n = \frac{1}{2}\int_{-D}^{D} d\epsilon \rho_0(\epsilon)[f(E_1(\epsilon)) + f(E_2(\epsilon))], \tag{6}$$

$$\frac{\Delta}{W} = \Delta \int_{-D}^{D} d\epsilon \rho_0(\epsilon)\left[\frac{f(E_1(\epsilon)) - f(E_2(\epsilon))}{2Q(\epsilon)}\right], \tag{7}$$

where $f(x)$ is the (doubled) Fermi function, $E_{1,2}(\epsilon) = Wn - \mu \mp Q(\epsilon)$, and $Q(\epsilon) = \sqrt{W^2\Delta^2 + \epsilon^2}$ [30,33]. The grand canonical potential has the form

$$\Omega = C - \frac{1}{\beta}\sum_{\alpha=1,2}\int d\epsilon \rho_0(\epsilon) \ln\{1 + \exp[-\beta E_\alpha(\epsilon)]\}, \tag{8}$$

with the C term defined previously, after Eq. (2).

The noninteracting ground state phase diagram of the model [see Fig. 1(a)] shows the existence of two phases, namely a Fermi liquid metallic state (FL) and a half-filled, i.e., $n = 1$, charge-ordered insulator (HCOI). The transition between these two states is of first order, characterized by a discontinuous change of both the occupation n and the polarization Δ and phase separation for a definite range of n is present. For $U = 0$ and any $n \neq 1$ a charge-ordered metallic (COM) phase is not stable, i.e., $\partial n/\partial\mu < 0$ [62–68]. In this limit model (1) is equivalent with the spinless fermion model [62–68].

B. Atomic limit

In the $D = 0$ limit model (2) has been studied in great detail (see for example Refs. [69,70,70–74] and references therein). Here, we briefly review the rigorous results in the limit $z \to +\infty$ obtained using a variational approach, which treats the on-site U interaction exactly and the intersite W interactions within the mean-field approximation [69,72,74]. The ground state phase diagram for $D = 0$ is reported in Fig. 1(b).

The diagram features different charge-ordered insulating (COI) phases: a quarter-filled one (QCOI) ($n = 0.5$) and a HCOI solution. In addition two nonordered phases are present: a band insulator for $n = 0$ and a Mott-insulating (MI) phase at $n = 1$. Notice that although all transitions

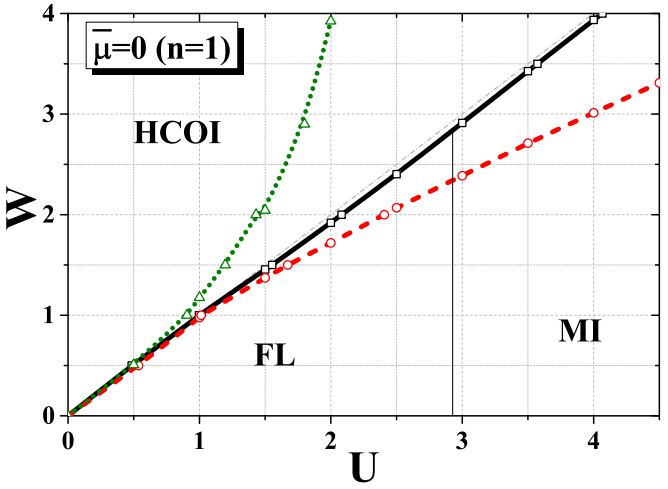

FIG. 2. The ground state phase diagram in the W-U plane at half filling, i.e., $n = 1$. The solid line (black) at $W/U \simeq 1$ denotes the first-order transition separating the half-filled charge-ordered insulator (HCOI) from the nonordered phase. The latter includes a Fermi liquid (FL) metal and a Mott insulator (MI). The dashed line (red) delimits the region of metastability of the HCOI phase. Similarly the dotted line (green) indicates the region of metastability for the nonordered phases.

are discontinuous, the homogeneous phases occurring for fixed $n \neq 0.5$ or $n \neq 1$ are degenerated with phase separated states. Finite-temperature or longer-range intersite interactions however can remove this degeneracy [72,74].

III. PHASE DIAGRAM

We now turn our attention to the combined effect of the local and nonlocal interactions in model (2). We first investigated the case of the half filling, i.e., $\bar{\mu} = 0$ and $n = 1$. The $T = 0$ phase diagram in the U-W plane is reported in Fig. 2. The figure shows the existence in this regime of three distinct solutions. A HCOI is found for $U \lesssim W$ separated from the normal (nonordered) solution by a boundary line just below $W/U = 1$. The normal solution includes a FL metal at small U and a MI for large enough U. In our approach the FL-MI transition line is roughly independent from W. More accurate calculations, taking into account the nonlocal interaction beyond the mean-field level, have pointed out a weak dependence of the Mott transition line on the W interaction [52]. In the same diagram of Fig. 2 we also denote the region of metastability of the ordered and normal phases enclosed within two spinodal lines. While the HCOI phase extends little into the normal region, we observe that the coexistence region of the nonordered solution in the HCOI phase rapidly grows with increasing W, already for small values of U.

We shall now study the competition of strong correlation and charge ordering at finite values of the chemical potential $\bar{\mu}$. Our main result is summarized by the phase diagrams in the plane W-$\bar{\mu}$, reported in Fig. 3. The figure shows the evolution of the diagrams upon increasing the local correlation strength U. For a finite value of U we observe the presence of two additional phases with respect to the noninteracting regime

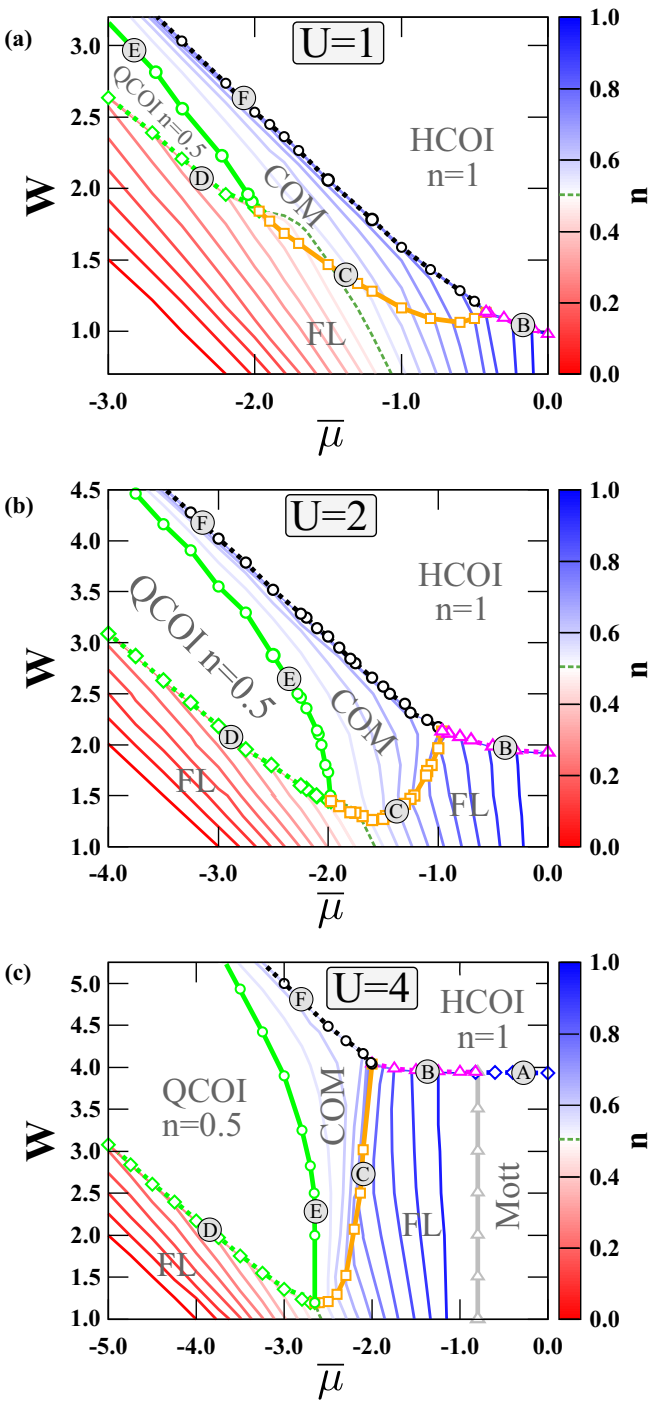

FIG. 3. The $T = 0$ phase diagrams in the W-$\bar{\mu}$ plane for increasing local interactions: $U = 1,2,4$ (as labeled). The diagrams show the existence of a Fermi liquid (FL) metallic state at small W, of a charge-ordered metal (COM) for incommensurate occupation, a quarter-filled (QCOI) and a half-filled charge-ordered insulator (HCOI), a Mott insulating phase near the $\bar{\mu} = 0$. The solid lines (C and E) correspond to continuous phase transitions, whereas the dotted lines (A, B, D, and F) correspond to first-order ones. The letters associated to the boundary lines correspond to the paragraphs in Sec. IV. The other solid lines are the isodensity lines, colored according to the value of the total density n in the right column. The dashed line is for $n = 0.5$.

[cf. Fig. 1(a)], i.e., a charge-ordered metal (COM) and a quarter-filled charge-ordered insulator (QCOI), i.e., $n = 0.5$ [Figs. 3(a) and 3(b)].

Similarly to the results obtained in Refs. [16,17], at quarter filling the system undergoes a sequence of transitions as a function of increasing W, namely a continuous one from the FL metal to the COM followed by a second-order transition to the QCOI. The evolution of the system for $n = 0.5$ is indicated by the dotted line in Fig. 3.

The COM and QCOI phases separate the HCOI solution from the Fermi liquid metallic state. A change in the chemical potential $\bar{\mu}$ first destabilizes the HCOI towards the charge-ordered metal, occurring for $n < 1$ and for intermediate values of the nonlocal interaction W. With further decreasing of the chemical potential the system can reach the second charge-ordered insulating state, i.e., the QCOI.

The slope of the boundary line of the HCOI is governed by the width of the gap, which is linear in W. Upon increasing the strength of the local correlation we observe a substantial modification of the COM and the QCOI regions, with the latter increasing its extension. This is in agreement with the fact that for larger values of U it becomes easier for the depleted system to pin the occupation of a single sublattice to a commensurate value, which ultimately favors the formation of a charge-ordered solution. Correspondingly the HCOI region moves towards higher values of W, with the FL-HCOI transition always occurring at $U \simeq W$. Interestingly, the evolution of the boundary lines separating the two metallic phases (Fermi liquid and charge ordered) is not monotonic in U (see Fig. 3). The negative slope of the boundary line in the weak-interaction regime [Fig. 3(a)] is progressively transformed into a large positive one at strong coupling [Fig. 3(c)]. This change follows directly the evolution of the total occupation behavior as outlined by the isodensity lines in the diagrams of Fig. 3. By increasing the strength of the local interaction U, the occupation near the FL-COM boundary line becomes nearly independent of W. This behavior is associated with the more localized nature of the metallic state (at small doping) near the Mott-insulating phase, occurring for $U \gtrsim 2.92$ near the $\bar{\mu} = 0$ point [see Fig. 3(c)].

IV. PHASE TRANSITIONS

In this section we discuss the properties of the transitions among the different phases of the system. To this end, we shall introduce other distinctive quantities, beside the aforementioned charge polarization Δ, i.e., the spectral densities at the Fermi level, $\rho_\alpha(0) = -\frac{1}{\pi}\mathrm{Im}G_{\mathrm{loc},\alpha}(\omega = 0)$, and the renormalization constants $Z_\alpha = (1 - \frac{\partial \Sigma_\alpha(\omega)}{\partial \omega}_{|\omega=0})^{-1}$ $(\alpha = A, B)$.

A. The MI-HCOI transition

To start with we discuss the transition between the Mott insulator and the HCOI [see Fig. 3(c)]. This transition occurs between two phases at half filling $(n = 1)$ and for a large enough value of U in order to guarantee the existence of the Mott insulator. The behavior of the charge polarization Δ as a function of the nonlocal interaction strength W is reported in Fig. 4(a). The evolution of the order parameter

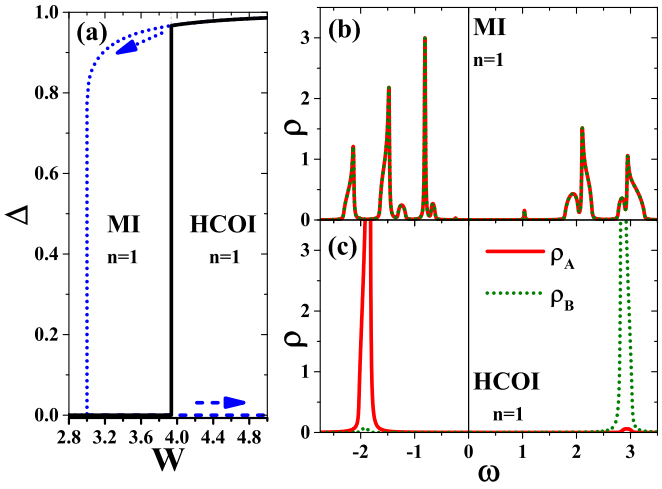

FIG. 4. The behavior of quantities in the neighborhood of the MI-HCOI boundary. (a) Δ as a function of W for $U = 4$ and $\bar{\mu} = -0.5$. The solid, dashed, and dotted lines correspond to stable, metastable MI, and metastable HCOI solutions, respectively. (b) Spectral densities for $W = 3.6$ (MI, $n = 1$). (c) Spectral densities for $W = 4.4$ (HCOI, $n = 1$). Solid and dotted lines correspond to different sublattices [in panels (b) and (c)]. The Fermi level is at $\omega = 0$.

exhibits a discontinuity at the transition point, indicating its first-order nature as expected for a symmetry-related transition between two insulating states of different origin. Accordingly, the transition shows a remarkable hysteresis of Δ, associated with the existence of metastable phases on both sides of the transition [see Fig. 4(a)]. The metastable Mott-insulating region extends to large values of W even beyond the limit of the figure.

In panels (b) and (c) of Fig. 4 we compare the spectral densities $\rho_\alpha(\omega) = -\frac{1}{\pi}\mathrm{Im}G_{\mathrm{loc},\alpha}(\omega)$ $(\alpha = A, B)$ in the two phases. In the Mott region the spectral functions are characterized by the two contributions at high energy, separated by a gap of the order U, the hallmark of the Mott nature of the solution. The asymmetry of the spectrum is associated with the finite value of the nonlocal term W.

In the HCOI region [see Fig. 4(c)] the spectral density is characterized by a band gap, separating the completely filled sublattice A $(n_A \approx 2)$ from the empty sublattice B $(n_B \approx 0)$. The gap is related to charge order phenomenon and has a width of $\simeq 2(W - U/2)\Delta$. Because of its mean-field nature with respect to symmetry-breaking transition, the DMFT description of charge-ordered state closely follows the mean-field solution of the problem [62].

B. The FL-HCOI transition

At finite doping the system admits a transition between the Fermi liquid metal and the HCOI solution. Differently from the previous case this transition occurs between states at different fillings. The behavior of the order parameter Δ and the occupation n across the transition boundary is reported in Fig. 5(a). Both quantities exhibit an abrupt change at the transition. In particular, n evolves discontinuously from $n = 1$, in the ordered phase, to $n \approx 0.92 < 1$ in the normal metallic

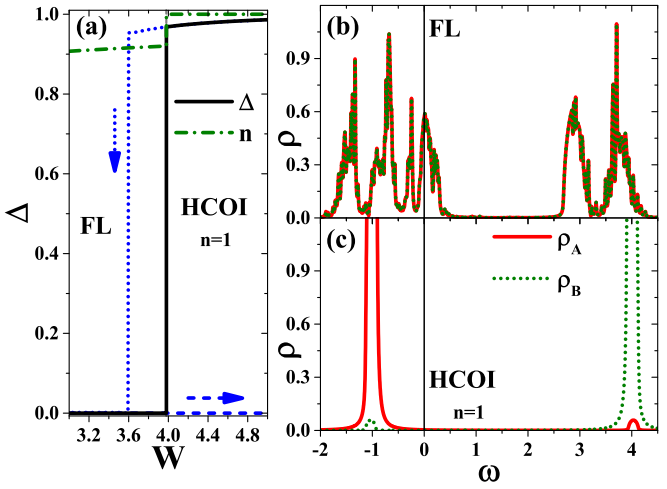

FIG. 5. The behavior of quantities in the neighborhood of the FL-HCOI boundary. (a) Δ (solid line) and n (dashed-dotted line) as a function of W for $U = 4$ and $\bar{\mu} = -1.5$. The dashed and dotted lines correspond to metastable FL and metastable HCOI solutions, respectively. (b) Spectral densities for $W/D = 3.6$ (FL). (c) Spectral densities for $W/D = 4.4$ (HCOI, $n = 1$). Solid and dotted lines correspond to different sublattices [in panels (b) and (c)]. The Fermi level is at $\omega = 0$.

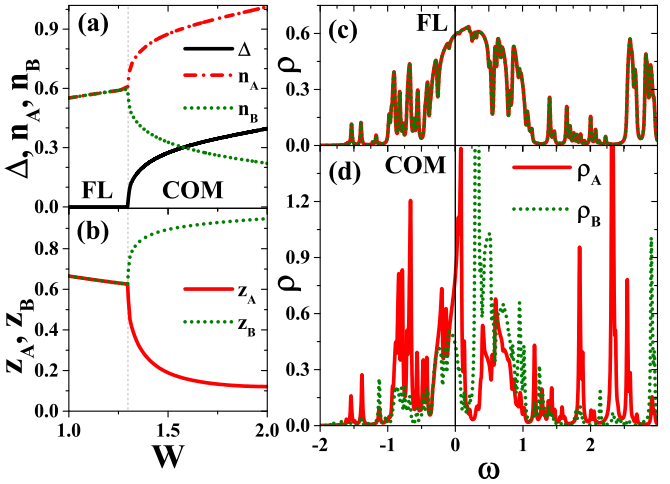

FIG. 6. The behavior of quantities in the neighborhood of the FL-COM boundary. (a) Δ (solid line), n_A (dashed-dotted line), and n_B (dotted line) as a function of W for $U/D = 2.0$ and $\bar{\mu}/D = -1.5$. (b) z_A (solid line) and z_B (dotted line) as a function of W for the same values of the other parameters. (c) Spectral densities for $W = 1.25$ (FL). (d) Spectral densities for $W = 1.35$ (COM). Solid and dotted lines correspond to different sublattices [in panels (c) and (d)]. The Fermi level is at $\omega = 0$.

region. The first-order character of the FL-HCOI transition is further underlined by the hysteresis of Δ. Analogously to the Mott phase, the region of metastability of the FL phase extends to large values of W (beyond the range of the figure).

The spectral functions of the two solutions for the $U = 4$ case are reported in Figs. 5(b) and 5(c). In the FL phase the spectral densities, identical for both sublattices $\rho_A(\omega) = \rho_B(\omega)$, have a finite weight at the Fermi level ($\omega = 0$) obtained by small doping ($\bar{\mu} = -1.5$) of the Mott-insulating solution. The quasiparticle resonance at the Fermi level flanks the lower Hubbard band, which in turn is separated by a gap of order U from the upper one. In panel (c) we show the spectral densities for the HCOI phase. The rigid shift with respect to Fig. 4(c) is due the different value of the chemical potential. However, the properties of this phase remain unchanged.

C. The FL-COM transition

Similarly, the FL metal can be destabilized towards the COM phase by either increasing the nonlocal interaction W or the doping value. The symmetry-breaking transition relating these two phases at incommensurate filling is continuous, i.e., of second order. Further insight in the continuous character of the transition can be inferred from the behavior of the isodensity lines across the boundary line; see Fig. 3. Approaching the transition from both phases, the density evolves smoothly enabling the continuous formation/destruction of the charge polarization. The behavior of the densities $n_{A,B}$ and of the order parameter Δ as a function of W for $U = 2$ is reported in Fig. 6(a). Crossing the transition line (see the phase diagram in Fig. 3) by decreasing W from the COM solution, the order parameter Δ gets continuously reduced to zero. In proximity of the critical point $W = W_c$ the order parameter exhibits the characteristic square-root behavior $\Delta = (W - W_c)^{1/2}$ [see Fig. 6(a)] as expected from a mean-field description of the phase transition.

In the charge-ordered phase the unbalanced occupations in the two sublattices give rise to different degrees of correlation. We quantify this showing the behavior of the renormalization constants $Z_{A,B}$ across the phase transition in Fig. 6(b). In particular, the sublattice A becomes nearly half filled ($n_A \simeq 1$) while the other one B gets slightly depleted. Correspondingly $Z_A < Z_B$; i.e., the metallic state at A becomes significantly more correlated than the other sublattice.

The different nature of the metallic states at the two phases is also evident from the corresponding spectral functions, reported in Figs. 6(c) and 6(d). A large featureless spectral weight, reminiscent of the noninteracting (semielliptic) distribution, characterizes both sublattices in the FL phase. The effect of the large correlation U manifests itself in the contribution at high energy [Fig. 6(c)]. In the charge-ordered phase the two spectral functions show the formation of a tiny gap slightly away from the Fermi level ($\omega = 0$). The symmetry breaking associated with charge ordering is responsible for the opening of a small spectral gap. However, the charge unbalance at finite W between the two sublattices leads in this regime to a small doping with respect to the (ordered) insulating state, resulting in a finite spectral density at the Fermi level characteristic of a metallic state. In this regime the two sublattice distributions are nearly specular one with respect to another, with a relative shift of about $2W\Delta$. The strongly correlated nature of the sublattice A solution is further underlined by the narrow resonance at the Fermi level characterizing the spectral function at low energy [see Fig. 6(d)]. Likewise, precursors of the Hubbard bands are visible in the higher energy region.

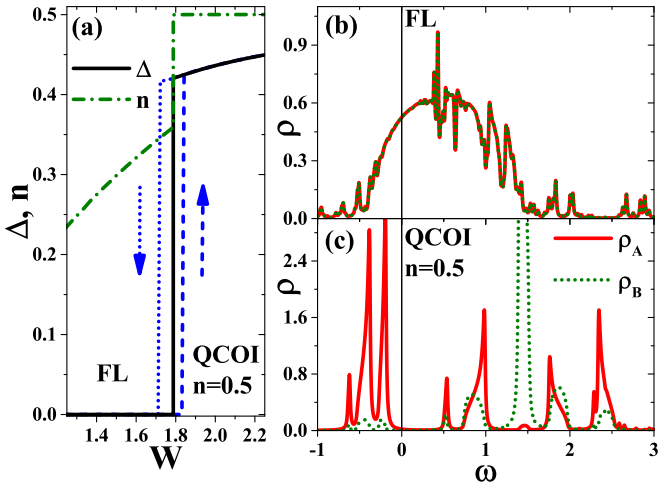

FIG. 7. The behavior of quantities in the neighborhood of the FL-QCOI boundary. (a) Δ (solid line) and n (dashed-dotted line) as a function of W for $U = 2.0$ and $\bar{\mu} = -2.5$. The dashed and dotted lines correspond to metastable FL and metastable QCOI solutions, respectively. (b) Spectral densities for $W = 1.70$ (FL). (c) Spectral densities for $W = 1.85$ (QCOI, $n = 0.5$). Solid and dotted lines correspond to different sublattices [in panels (b) and (c)]. The Fermi level is at $\omega = 0$.

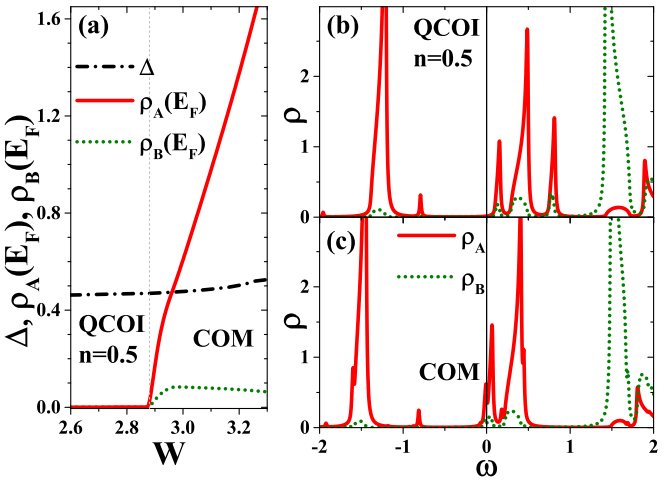

FIG. 8. The behavior of quantities in the neighborhood of the QCOI-COM boundary. (a) Δ (dashed-dotted line), $\rho_A(E_F)$ (solid line), and $\rho_B(E_F)$ (dotted line) as a function of W for $U = 2.0$ and $\bar{\mu} = -2.5$. (b) Spectral densities for $W = 2.75$ (QCOI, $n = 0.5$). (c) Spectral densities for $W = 3.00$ (COM). Solid and dotted lines correspond to different sublattices [in panels (b) and (c)]. The Fermi level is at $\omega = 0$.

D. The FL-QCOI transition

For even larger values of the chemical potential $\bar{\mu}$, i.e., doping, the effect of nonlocal interaction W is to transform the Fermi liquid metal directly into a QCOI. The transition occurs through the pinning of the occupation to a commensurate value for one sublattice with the concomitant opening of a charge-order gap, while the other sublattice becomes nearly empty. The discontinuous nature of the transition can be further appreciated by looking at the evolution of the isodensity lines near the boundary line. As reported in Fig. 3, near the transition the FL metal has a small occupation while the QCOI is pinned to $n = 0.5$. This prevents the continuous transformation of one state into the other and the only way to connect these two phases is through a first-order jump.

The behavior of the density n and of the order parameter Δ as a function of W across the transition is reported in Fig. 7(a). The occupation n undergoes a jump to $n = 0.5$ for a critical value of the nonlocal interaction $W = W_c$. At the critical point the charge polarization Δ suddenly acquires a finite value. The figure also shows the hysteresis cycle of the order parameter, demonstrating the first-order nature of this transition.

In panels (b) and (c) of the figure we report the evolution of the spectral functions across the phase transition. In the FL phase [see Fig. 7(b)], the distribution is characterized by a large featureless spectrum. In this low-density regime and for small W the effects of the local correlation are rather weak. Entering the QCOI region both spectral functions exhibit a gap of the order of $\mathrm{Max}\{2W\Delta, U\}$ at the Fermi level, associated with the charge order and Mott localization occurring in the system. The spectral weight of the sublattice B is located above the Fermi level, corresponding to an almost depleted regime, while the other sublattice is nearly half filled due to intersite repulsion W.

The interplay between both U and W interaction has a strong impact on this phase and, as discussed in Sec. III and Ref. [17], they both contribute to stabilizing the QCOI phase. Thus, the occurrence of the QCOI phase is associated with the conventional Mott scenario for the localization of the electrons in nearly half-filled sublattice A, whereas almost empty sublattice B is rather a band insulator [17].

E. The QCOI-COM transition

The charge-ordered insulating phase at quarter filling can be destabilized by either reducing the doping (i.e., reducing the chemical potential) or increasing W. The resulting insulator-to-metal transition however occurs without destroying the long-range charge order. In Fig. 8(a) we demonstrate this by tuning the nonlocal interaction W, driving the QCOI into a COM state. In this figure we show that charge polarization Δ remains finite across the transition. We characterize the metallization process through the behavior of the spectral weights at the Fermi level $\rho_{A,B}(E_F \equiv 0)$ across the transition. These quantities show a continuous evolution, corresponding to a second-order phase transition. In particular, the sublattice A, which is near the half-filling occupation, rapidly gains a substantial amount of spectral weight at Fermi level, developing continuously into a strongly correlated metal, i.e., $Z_A \simeq 0$ (not shown in the figure). This is in agreement with the Wigner-Mott transition scenario for the electrons at the sublattice A [16,17].

The spectral distributions across the transition are reported in Figs. 8(b) and 8(c). The two cases are characterized by the presence of a large charge-order gap. Within our solution, increasing the interaction term W causes a small change of the chemical potential, which is sufficient to destabilize the charge-ordered insulator into a metallic state. However, in the presence of sufficiently strong local and nonlocal correlation

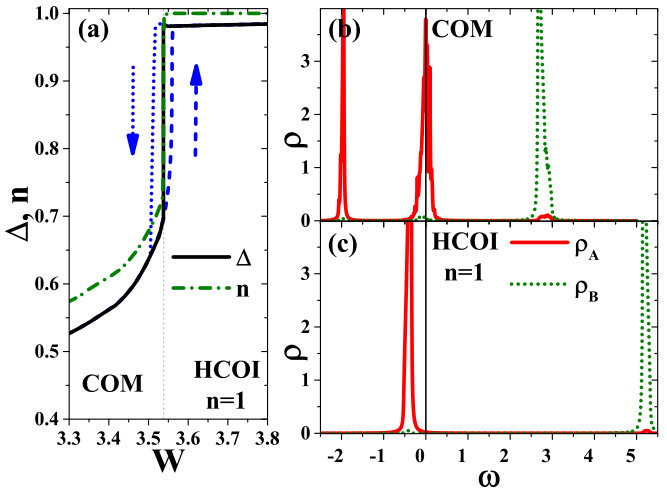

FIG. 9. The behavior of quantities in the neighborhood of the COM-HCOI boundary. (a) Δ (solid line) and n (dashed-dotted line) as a function of W for $U = 2.0$, $\bar{\mu} = -2.5$. The dashed and dotted lines correspond to metastable COM and metastable HCOI solutions, respectively. (b) Spectral densities for $W = 3.5$ (COM). (c) Spectral densities for $W = 3.8$ (HCOI, $n = 1$). Solid and dotted lines correspond to different sublattices [in panels (b) and (c)]. $\omega = 0$ corresponds to the Fermi level.

a small doping is not enough to suppress completely the long-range ordering, leading to the formation of the COM phase.

F. The COM-HCOI transition

We finally discuss the properties of the transition from the COM state to the HCOI phase. In Fig. 9(a) we report the behavior as a function of the interaction W of both the total density n and the charge polarization Δ across the transition line. Differently from the COM-QCOI case discussed previously, the transition from the charge-ordered metallic state to the HCOI has a first-order character. As reported in the figure at the critical point the total density jumps to the $n = 1$ value. Correspondingly, the order parameter discontinuously reaches its maximum value. The hysteresis of this quantity is also reported in the figure.

The spectral densities across the transition are shown in Figs. 9(b) and 9(c). The evolution of the spectra reveals that the metal-insulator transition is driven by a shift of the spectral weight below the Fermi level; i.e., the interaction W drives a shift in the chemical potential increasing the total occupation and a concomitant transfer of the spectral weight. In this regime the large value of W maintains the long-range charge order. The HCOI spectrum displays the distinctive features already discussed in the previous sections.

V. CONCLUSIONS

In this work we studied the competition between local and nonlocal electronic interaction within the paradigmatic extended Hubbard model. We solved the model nonperturbatively using the dynamical mean-field theory, with a Lanczos exact diagonalization technique. In particular we thoroughly investigated the interplay of charge ordering and Mott physics as a function of the chemical potential which in turn controls the particle density. We determined the zero-temperature phase diagram as a function of the nonlocal interaction W and chemical potential $\bar{\mu}$. For any value of local correlation U we reported the existence of both an insulating charge-ordered solution at quarter filling and an incommensurate charge-ordered metal. These two phases, which have no counterpart in the noninteracting regime, get stabilized by the interplay of local and longer-range interactions. The evolution of the phase diagram as a function of U has shown the increasing stability of the quarter-filled charge-ordered solution.

We studied in detail the nature and the properties of the different phase transitions occurring among the multiple phases of the system. In particular we unveiled the characteristics of the continuous metal-insulator transition separating the charge-ordered metal and the $n = 0.5$ insulator, which extends to the incommensurate case previous results available in the recent literature. Moreover, we showed that the small-W Fermi liquid metal is separated from the charge-ordered metallic state by a continuous transition and from the quarter-filled charge-ordered insulator by a first-order one. The analysis of the isodensity lines enabled us to associate the difference in the transition character to distinct behavior of the occupation in the two regimes. Thus, for example, the incommensurate filling of the charge-ordered metal can be continuously connected with the Fermi liquid state through the progressive reduction of the charge polarization. On the contrary in the large-doping regime, the severe difference in the occupation between the quarter-filled charge-ordered insulator and the almost empty Fermi liquid leaves room only for a first-order phase transition.

Although the simple nature the extended Hubbard model cannot be regarded as a realistic or quantitatively accurate representation of the real system, its solution in a nonperturbative framework allows us to shed light on the microscopic mechanism behind several experimental observations. Notice also that the immense development of experimental techniques in cold atomic Fermi gases on the optical lattices in the last years has opened new opportunities for research of strongly correlated systems and beyond. The ability to precisely control the interactions via Feshbach resonances [75–77] sets new perspectives for experimental realization and study of many different theoretically well-described system, in particular various nonstandard Hubbard models (for review see, e.g., Refs. [78,79]).

Our study demonstrates how the tendency to charge ordering favors and strengthens the transformation of conduction electrons into localized particles in the presence of long-range charge order. The analysis of the phase transitions and the destruction of the charge ordering at an arbitrary filling can be useful to understand recent experiments on the 2D electron gas from deposed liquid He^3 on a substrate, which corresponds to incommensurate density [80–85].

ACKNOWLEDGMENTS

K.J.K. thanks SISSA for the hospitality during his six month research stay in Trieste in 2015. A.A. and M.C. acknowledge financial support from the European Research Council under FPO7 Starting Independent Research Grant No. 240524 "SUPERBAD." A.A. also acknowledges support from the

European Union, Seventh Framework Programme FP7, under Grant No. 280555 "GO FAST" and under H2020 Framework Programme, ERC Advanced Grant No. 692670 "FIRSTORM" for part of this work. K.J.K. was supported by National Science Centre (NCN, Poland)–ETIUDA 1 Programme, Grant No. DEC-2013/08/T/ST3/00012 in years 2013–2015.

[1] P. Fulde, P. Thalmeier, and G. Zwicknagl, Strongly correlated electrons, in *Solid State Physics Advances in Research and Applications*, Solid State Physics, Vol. 60, edited by H. Ehrenreich and F. Spaepen (Academic Press, San Diego, 2006), pp. 1–180.

[2] V. Anisimov and Y. Izyumov, *Electronic Structure of Strongly Correlated Materials*, Springer Series in Solid-State Sciences, Vol. 163 (Springer-Verlag, Berlin, 2010).

[3] J. Hubbard, Electron correlations in narrow energy bands, Proc. R. Soc. London **276**, 238 (1963).

[4] D. R. Penn, Stability theory of the magnetic phases for a simple model of the transition metals, Phys. Rev. **142**, 350 (1966).

[5] J. Spałek, A. Datta, and J. M. Honig, Discontinuous Metal-Insulator Transitions and Fermi-Liquid Behavior of Correlated Electrons, Phys. Rev. Lett. **59**, 728 (1987).

[6] A. Georges, G. Kotliar, W. Krauth, and M. J. Rozenberg, Dynamical mean-field theory of strongly correlated fermion systems and the limit of infinite dimensions, Rev. Mod. Phys. **68**, 13 (1996).

[7] F. Gebhard, *The Mott Metal-Insulator Transition: Models and Methods*, Springer Tracts in Modern Physics, Vol. 137 (Springer-Verlag, Berlin, 1997).

[8] A. Montorsi (ed.), *The Hubbard Model: A Collection of Reprints* (World Scientific, Singapore, 1992).

[9] J. Vučičević, D. Tanasković, M. J. Rozenberg, and V. Dobrosavljević, Bad-Metal Behavior Reveals Mott Quantum Criticality in Doped Hubbard Models, Phys. Rev. Lett. **114**, 246402 (2015).

[10] J. Sólyom, Wigner crystals: New realizations of an old idea, EPJ Web Conf. **78**, 01009 (2014).

[11] E. Wigner, On the interaction of electrons in metals, Phys. Rev. **46**, 1002 (1934).

[12] E. Y. Andrei, G. Deville, D. C. Glattli, F. I. B. Williams, E. Paris, and B. Etienne, Observation of a Magnetically Induced Wigner Solid, Phys. Rev. Lett. **60**, 2765 (1988).

[13] Y. Hanein, U. Meirav, D. Shahar, C. C. Li, D. C. Tsui, and H. Shtrikman, The Metalliclike Conductivity of a Two-Dimensional Hole System, Phys. Rev. Lett. **80**, 1288 (1998).

[14] S. V. Kravchenko and M. P. Sarachik, Metal-insulator transition in two-dimensional electron systems, Rep. Prog. Phys. **67**, 1 (2004).

[15] S. Pankov and V. Dobrosavljević, Self-doping instability of the Wigner-Mott insulator, Phys. Rev. B **77**, 085104 (2008).

[16] A. Camjayi, K. Haule, V. Dobrosavljević, and G. Kotliar, Coulomb correlations and the Wigner-Mott transition, Nat. Phys. **4**, 932 (2008).

[17] A. Amaricci, A. Camjayi, K. Haule, G. Kotliar, D. Tanasković, and V. Dobrosavljević, Extended Hubbard model: Charge ordering and Wigner-Mott transition, Phys. Rev. B **82**, 155102 (2010).

[18] E. Morosan, H. W. Zandbergen, B. S. Dennis, J. W. G. Bos, Y. Onose, T. Klimczuk, A. P. Ramirez, N. P. Ong, and R. J. Cava, Superconductivity in Cu_xTiSe_2, Nat. Phys. **2**, 544 (2006).

[19] A. M. Novello, B. Hildebrand, A. Scarfato, C. Didiot, G. Monney, A. Ubaldini, H. Berger, D. R. Bowler, P. Aebi, and Ch. Renner, Scanning tunneling microscopy of the charge density wave in $1T$-$TiSe_2$ in the presence of single atom defects, Phys. Rev. B **92**, 081101(R) (2015).

[20] M. Imada, A. Fujimori, and Y. Tokura, Metal-insulator transitions, Rev. Mod. Phys. **70**, 1039 (1998).

[21] Ch. Renner, G. Aeppli, B.-G. Kim, Y.-A. Soh, and S.-W. Cheong, Atomic-scale images of charge ordering in a mixed-valence manganite, Nature (London) **416**, 518 (2002).

[22] T. Goto and B. Lüthi, Charge ordering, charge fluctuations and lattice effects in strongly correlated electron systems, Adv. Phys. **52**, 67 (2003).

[23] E. Dagotto, T. Hotta, and A. Moreo, Colossal magnetoresistant materials: The key role of phase separation, Phys. Rep. **344**, 1 (2001).

[24] E. H. da Silva Neto, R. Comin, F. He, R. Sutarto, Y. Jiang, R. L. Greene, G. A. Sawatzky, and A. Damascelli, Charge ordering in the electron-doped superconductor $Nd_{2-x}Ce_xCuO_4$, Science **347**, 282 (2015).

[25] H. Seo, C. Hotta, and H. Fukuyama, Toward systematic understanding of diversity of electronic properties in low-dimensional molecular solids, Chem. Rev. **104**, 5005 (2004).

[26] D. Jérome, Organic conductors: From charge density wave TTF-TCNQ to superconducting $(TMTSF)_2PF_6$, Chem. Rev. **104**, 5565 (2004).

[27] C. Bourbonnais and D. Jérome, Interacting electrons in quasi-one-dimensional organic superconductors, in *The Physics of Organic Superconductors and Conductors*, edited by A. Lebed (Springer, Berlin, 2008), pp. 357–412.

[28] A. Ochiai, T. Suzuki, and T. Kasuya, Heavy fermion behavior in extremely low carrier concentration system Yb_4As_3, J. Phys. Soc. Jpn. **59**, 4129 (1990).

[29] P. Fulde, B. Schmidt, and P. Thalmeier, Theoretical model for the semi-metal Yb_4As_3, Europhys. Lett. **31**, 323 (1995).

[30] S. Robaszkiewicz, Electron-charge ordering and insulator-metal transition in an extended Hubbard model, Acta Phys. Pol. A **45**, 289 (1974).

[31] H.Q. Lin, D.K. Campbell, and R.T. Clay, Broken symmetries in the one-dimensional extended Hubbard model, Chin. J. Phys. **38**, 1 (2000).

[32] A.T. Hoang and P. Thalmeier, Coherent potential approximation for charge ordering in the extended Hubbard model, J. Phys.: Condens. Matter **14**, 6639 (2002).

[33] S. Robaszkiewicz, The charge-ordered state in an extended Hubbard model, Phys. Status Solidi B **59**, K63 (1973).

[34] R. Micnas, J. Ranninger, and S. Robaszkiewicz, Superconductivity in narrow-band systems with local nonretarded attractive interactions, Rev. Mod. Phys. **62**, 113 (1990).

[35] K. Rościszewski and A. M. Oleś, Charge order in the extended Hubbard model, J. Phys.: Condens. Matter **15**, 8363 (2003).

[36] J. E. Hirsch, Charge-Density-Wave to Spin-Density-Wave Transition in the Extended Hubbard Model, Phys. Rev. Lett. **53**, 2327 (1984).

[37] H. Q. Lin and J. E. Hirsch, Condensation transition in the one-dimensional extended Hubbard model, Phys. Rev. B **33**, 8155 (1986).
[38] R. T. Clay, A. W. Sandvik, and D. K. Campbell, Possible exotic phases in the one-dimensional extended Hubbard model, Phys. Rev. B **59**, 4665 (1999).
[39] M. Aichhorn, H. G. Evertz, W. von der Linden, and M. Potthoff, Charge ordering in extended Hubbard models: Variational cluster approach, Phys. Rev. B **70**, 235107 (2004).
[40] K. Penc and F. Mila, Phase diagram of the one-dimensional extended Hubbard model with attractive and/or repulsive interactions at quarter filling, Phys. Rev. B **49**, 9670 (1994).
[41] M. Calandra, J. Merino, and R. H. McKenzie, Metal-insulator transition and charge ordering in the extended Hubbard model at one-quarter filling, Phys. Rev. B **66**, 195102 (2002).
[42] J. Merino, H. Seo, and M. Ogata, Quantum melting of charge order due to frustration in two-dimensional quarter-filled systems, Phys. Rev. B **71**, 125111 (2005).
[43] S. Fratini and J. Merino, Unconventional metallic conduction in two-dimensional Hubbard-Wigner lattices, Phys. Rev. B **80**, 165110 (2009).
[44] B. Davoudi and A.-M. S. Tremblay, Nearest-neighbor repulsion and competing charge and spin order in the extended Hubbard model, Phys. Rev. B **74**, 035113 (2006).
[45] M. Vojta, R. E. Hetzel, and R. M. Noack, Charge-order transition in the extended Hubbard model on a two-leg ladder, Phys. Rev. B **60**, R8417(R) (1999).
[46] M. Vojta, A. Hübsch, and R. M. Noack, Phase diagram of the quarter-filled extended Hubbard model on a two-leg ladder, Phys. Rev. B **63**, 045105 (2001).
[47] R. Pietig, R. Bulla, and S. Blawid, Reentrant Charge Order Transition in the Extended Hubbard Model, Phys. Rev. Lett. **82**, 4046 (1999).
[48] N.-H. Tong, S.-Q. Shen, and R. Bulla, Charge ordering and phase separation in the infinite dimensional extended Hubbard model, Phys. Rev. B **70**, 085118 (2004).
[49] J. Merino, A. Ralko, and S. Fratini, Emergent Heavy Fermion Behavior at the Wigner-Mott Transition, Phys. Rev. Lett. **111**, 126403 (2013).
[50] J. Merino, Nonlocal Coulomb Correlations in Metals Close to a Charge Order Insulator Transition, Phys. Rev. Lett. **99**, 036404 (2007).
[51] T. Ayral, P. Werner, and S. Biermann, Spectral Properties of Correlated Materials: Local Vertex and Nonlocal Two-Particle Correlations from Combined GW and Dynamical Mean Field Theory, Phys. Rev. Lett. **109**, 226401 (2012).
[52] T. Ayral, S. Biermann, and P. Werner, Screening and nonlocal correlations in the extended Hubbard model from self-consistent combined GW and dynamical mean field theory, Phys. Rev. B **87**, 125149 (2013).
[53] L. Huang, T. Ayral, S. Biermann, and P. Werner, Extended dynamical mean-field study of the Hubbard model with long-range interactions, Phys. Rev. B **90**, 195114 (2014).
[54] H. Hafermann, E. G. C. P. van Loon, M. I. Katsnelson, A. I. Lichtenstein, and O. Parcollet, Collective charge excitations of strongly correlated electrons, vertex corrections, and gauge invariance, Phys. Rev. B **90**, 235105 (2014).
[55] E. G. C. P. van Loon, A. I. Lichtenstein, M. I. Katsnelson, O. Parcollet, and H. Hafermann, Beyond extended dynamical mean-field theory: Dual boson approach to the two-dimensional extended Hubbard model, Phys. Rev. B **90**, 235135 (2014).
[56] C. Février, S. Fratini, and A. Ralko, Multiorbital kinetic effects on charge ordering of frustrated electrons on the triangular lattice, Phys. Rev. B **91**, 245111 (2015).
[57] A. Ralko, J. Merino, and S. Fratini, Pinball liquid phase from Hund's coupling in frustrated transition-metal oxides, Phys. Rev. B **91**, 165139 (2015).
[58] W. Metzner and D. Vollhardt, Correlated Lattice Fermions in $d = \infty$ Dimensions, Phys. Rev. Lett. **62**, 324 (1989).
[59] E. Müller-Hartmann, Correlated fermions on a lattice in high dimensions, Z. Phys. B **74**, 507 (1989).
[60] M. Caffarel and W. Krauth, Exact Diagonalization Approach to Correlated Fermions in Infinite Dimensions: Mott Transition and Superconductivity, Phys. Rev. Lett. **72**, 1545 (1994).
[61] C. Weber, A. Amaricci, M. Capone, and P. B. Littlewood, Augmented hybrid exact-diagonalization solver for dynamical mean field theory, Phys. Rev. B **86**, 115136 (2012).
[62] R. Vlaming, G. S. Uhrig, and D. Vollhardt, Anomalous effects in interacting spinless fermion systems with local disorder, J. Phys.: Condens. Matter **4**, 7773 (1992).
[63] G. S. Uhrig and R. Vlaming, Interacting spinless fermions with disorder: The Mott transition for infinite coordination number, J. Phys.: Condens. Matter **5**, 2561 (1993).
[64] G. S. Uhrig and R. Vlaming, Inhibition of Phase Separation and Appearance of New Phases for Interacting Spinless Fermions, Phys. Rev. Lett. **71**, 271 (1993).
[65] G. S. Uhrig and R. Vlaming, Zero and finite temperature phase diagram of the spinless fermion model in infinite dimensions, Ann. Phys. **507**, 778 (1995).
[66] W. R. Czart, S. Robaszkiewicz, and B. Tobijaszewska, Charge ordering and phase separations in the spinless fermion model with repulsive intersite interaction, Acta Phys. Pol. A **114**, 129 (2008).
[67] W. R. Czart, P. R. Grzybowski, M. Nogala, and S. Robaszkiewicz, Effects of frustrating hopping on charge ordered states in itinerant fermion systems for arbitrary concentration in 2D lattice, Acta Phys. Pol. A **121**, 828 (2012).
[68] W.R. Czart, P. R. Grzybowski, M. Nogala, and S. Robaszkiewicz, Charge orderings and phase separations in itinerant fermion systems at half filling, Acta Phys. Pol. A **121**, 1042 (2012).
[69] R. Micnas, S. Robaszkiewicz, and K. A. Chao, Multicritical behavior of the extended Hubbard model in the zero-bandwidth limit, Phys. Rev. B **29**, 2784 (1984).
[70] F. Mancini and F. P. Mancini, One-dimensional extended Hubbard model in the atomic limit, Phys. Rev. E **77**, 061120 (2008).
[71] G. Ganzenmüller and G. Pawłowski, Flat histogram Monte Carlo sampling for mechanical variables and conjugate thermodynamic fields with example applications to strongly correlated electronic systems, Phys. Rev. E **78**, 036703 (2008).
[72] K. Kapcia and S. Robaszkiewicz, The effects of the next-nearest-neighbour density-density interaction in the atomic limit of the extended Hubbard model, J. Phys.: Condens. Matter **23**, 105601 (2011).
[73] F. Mancini, E. Plekhanov, and G. Sica, Exact solution of the 1D Hubbard model with NN and NNN interactions in the narrow-band limit, Eur. Phys. J. B **86**, 408 (2013).

[74] K. J. Kapcia and S. Robaszkiewicz, On the phase diagram of the extended Hubbard model with intersite density-density interactions in the atomic limit, Physica A **461**, 487 (2016).

[75] P. O. Fedichev, Yu. Kagan, G. V. Shlyapnikov, and J. T. M. Walraven, Influence of Nearly Resonant Light on the Scattering Length in Low-Temperature Atomic Gases, Phys. Rev. Lett. **77**, 2913 (1996).

[76] G. B. Partridge, W. Li, R. I. Kamar, Y.-a. Liao, and R. G. Hulet, Pairing and phase separation in a polarized Fermi gas, Science **311**, 503 (2006).

[77] C. H. Schunck, Y. Shin, A. Schirotzek, M. W. Zwierlein, and W. Ketterle, Pairing without superfluidity: The ground state of an imbalanced Fermi mixture, Science **316**, 867 (2007).

[78] I. M. Georgescu, S. Ashhab, and F. Nori, Quantum simulation, Rev. Mod. Phys. **86**, 153 (2014).

[79] O. Dutta, M. Gajda, P. Hauke, M. Lewenstein, D.-S. Lühmann, B. A. Malomed, T. Sowiński, and J. Zakrzewski, Non-standard Hubbard models in optical lattices: A review, Rep. Prog. Phys. **78**, 066001 (2015).

[80] E. Y. Andrei (ed.), *Two-Dimensional Electron Systems on Helium and other Cryogenic Substrates*, Physics and Chemistry of Materials with Low-Dimensional Structures, Vol. 19 (Springer Netherlands, 1997).

[81] M. Haque, I. Paul, and S. Pankov, Structural transition of a Wigner crystal on a liquid substrate, Phys. Rev. B **68**, 045427 (2003).

[82] D. Konstantinov and K. Kono, Novel Radiation-Induced Magnetoresistance Oscillations in a Nondegenerate Two-Dimensional Electron System on Liquid Helium, Phys. Rev. Lett. **103**, 266808 (2009).

[83] L. V. Levitin, R. G. Bennett, E. V. Surovtsev, J. M. Parpia, B. Cowan, A. J. Casey, and J. Saunders, Surface-Induced Order Parameter Distortion in Superfluid ^{3}He-B Measured by Nonlinear NMR, Phys. Rev. Lett. **111**, 235304 (2013).

[84] H. Yayama and Y. Yatsuyama, Mobility of 2D electrons on pure 4He and on 3He-4He dilute solution, J. Low Temp. Phys. **175**, 401 (2014).

[85] K. Aoyama, Stripe order in superfluid ^{3}He confined in narrow cylinders, Phys. Rev. B **89**, 140502 (2014).